Enhancing the Convex Analysis of Mixtures Technique for Estimating DCE-MRI Pharmacokinetic Parameters

Ibrahim Mohamed Ibrahim, Guoqiang Yu, Li Chen, and Yue Wang

***Abstract*—Dynamic-contrast enhanced magnetic resonance imaging (DCE-MRI) is a useful noninvasive tool for monitoring tumor angiogenesis and assessing therapeutic response. One major problem that prevents an accurate estimation of pharmacokinetic parameters is partial-volume effect (PVE). A multi-tissue compartmental modeling (CM) technique supported by convex analysis of mixtures (CAM) is used to overcome the PVE by clustering pixels and constructing a simplex whose vertices are of a single compartment type. CAM uses the identified pure-volume pixels to estimate the kinetics of the tissues under investigation. This paper reports an enhanced version of CAM-CM to identify pure-volume pixels more accurately. This includes the consideration of the neighborhood effect on each pixel and the use of a barycentric coordinate system to identify more pure-volume pixels and to test those identified by CAM. The enhanced CAM achieved root mean square error (RMSE) of 0.00348 ± 0.000019, lower than the RMSE of 0.05409 ± 0.00496 achieved by CAM.**

I. Introduction

Dynamic contrast-enhanced magnetic resonance imaging (DCE-MRI) is a noninvasive imaging tool for quantification of microvascular structure and function [1], with the goal of deriving some quantitative parameters that are related to the physiology of the region of interest and that are capable of describing the state of the microcirculation in that region [2], in an aid to monitor disease progress and assess treatment response [1], [3]. However, due to the discrete nature and finite bandwidth of image acquisition systems, a partial-volume effect (PVE) problem occurs, which is the result of signals from two or more tissues combining together to produce a single image concentration value within a pixel [4], with the effect of inaccurate estimation to the values of the pharmacokinetic parameters [3].

A compartmental modeling technique based on convex analysis of mixtures (CAM) [5] has been proposed to mitigate the PVE problem, in which the kinetics in each pixel is expressed as a nonnegative mixture of the cofounding tissues (compartments). CAM clusters pixels into a finite set of groups distributed within a simplex, with the simplex corners (vertices) being occupied by pure-volume pixels (pixels of just one tissue type that are PVE-free). Then, CAM identifies these pure-volume pixels and estimates the kinetic parameters values from these pixels, ignoring the pixels residing inside the simplex considering them as contaminated pixels with the PVE. The type of the simplex and hence the number of its vertices is determined based on the number of pure-volume compartments in the region under investigation (3 in our study representing the plasma input, fast flow, and slow flow).

Deeper analysis of CAM performance showed that it does not determine all the pure-volume pixels, and roughly speaking, its performance goes in either direction of these two ones based on the level of noise in the images:

- At low noise levels, CAM gets a smaller number of pixels- sometimes just one pixel- of each tissue type and defines them as pure-volume pixels. This means that there are many other pure-volume pixels defined as pixels with PVE.
- At high noise levels, CAM gets a larger number of pixels- sometimes larger than the number of all the ground-truth pure-volume pixels- and defines them as pure-volume pixels. This means that a number of pixels with PVE are mistakenly defined as pure-volume pixels, and also there may be some missed pure-volume pixels.

In this paper, two enhancements of CAM are proposed trying to get the more accurate number of pure-volume pixels. The first one is to compute the probabilistic memberships of each compartment at each pixel taking into account the neighborhood effect around that pixel. The second modification is to use the barycentric coordinate system (BCS) to get the contribution of each compartment for each pixel confined by the simplex convex hull.

II. Methods

A main step of the CAM technique to reduce the impact of noise/outlier data points and the computational complexity is to apply a multivariate pixel clustering, based on the standard finite normal mixtures (SFNM) with estimating its parameters using the expectation-maximization (EM) algorithm, to cluster the normalized pixel time series into a set of clusters that could be represented by:

$$p(X(i)) = \sum_{m=1}^{J} \pi_m \, g(X(i)|\mathbb{a}_m, \Sigma_{X,m}) + \sum_{m=J+1}^{M} \pi_m \, g(X(i)|\mu_{X,m}, \Sigma_{X,m}) \quad (1)$$

where the first term corresponds to the clusters of pure volume pixels ($m = 1, \dots, J$), the second term corresponds to the clusters of partial volume pixels ($m = J+1, \dots, M$), M is the total number of pixel clusters, $X(i)$ is the normalized concentration at pixel i, π_m is the mixing factor, $g(.)$ is the Gaussian kernel, $\mathbb{a}_m$ is the mean vector of the mth pure tissue

This work was supported by the Egyptian government through the VT-MENA Program.

Ibrahim Mohamed Ibrahim, Guoqiang Yu (corresponding author), and Yue Wang are with the Bradley Department of Electrical and Computer Engineering, Virginia Polytechnic Institute and State University, Arlington, VA 22203 USA (e-mail: i.m.ibrahim@vt.edu, yug@vt.edu, and yuewang@vt.edu).

Li Chen is with the Pediatric Oncology Branch, National Cancer Institute, National Institutes of Health, Gaithersburg, MD 20877, USA (e-mail: ahli1981@gmail.com).

compartment, $\mu_{X,m}$ and $\Sigma_{X,m}$ are the mean vector and covariance matrix of cluster *m*, respectively.

A. Neighborhood Weighted SFNM

The fact at our hand is that the tissue pixels have three classes (compartments) that are plasma input, fast flow, and slow flow. It was reported in [1] and [5] that the pixels of the fast flow class are found in the peripheral "rim" region of the tumor, and the slow flow class pixels are found in the inner "core" of the tumor. This could give an indication about the continuity (adjacency) of the pixels forming each class. But, due to PVE, concentration signals at some pixels may come from different compartments. Depending on a principle that the material is continuous, so it is natural to have the idea that the probability of the *m*th class of a pixel should be affected by the neighbors' *m*th class probabilities [6]. This means that the current voxel's *m*th class probability magnifies if the neighbors' *m*th class probabilities tend to 1, and that it decreases if the neighbors' *m*th class probabilities tend to 0.

We use the EM algorithm to estimate the model parameters $\theta = \{\pi_m, \mu_{X,m}, \Sigma_{X,m}, \forall m\}$ of (1). At each complete cycle of the algorithm, we start with an "old" set of parameter values θ. We first use these parameters in the E-step to evaluate the posterior probabilities z_{im}, at each pixel *i* and for cluster *m*, using Bayes theorem.

$$z_{im} = \frac{\pi_m g\left(X(i)\middle|\mu_{X,m}, \Sigma_{X,m}\right)}{\sum_{m'=1}^{M} \pi_{m'} g\left(X(i)\middle|\mu_{X,m'}, \Sigma_{X,m'}\right)}, m \in \{1, \dots, M\} \quad (2)$$

Incorporating the principle of material continuity affects the posterior probability in (2) by introducing a new term (*W*) representing the neighborhood effect:

$$z_{im} = \frac{\pi_m W_{im} g\left(X(i)\middle|\mu_{X,m}, \Sigma_{X,m}\right)}{\sum_{m'=1}^{M} \pi_{m'} W_{im'} g\left(X(i)\middle|\mu_{X,m'}, \Sigma_{X,m'}\right)} \quad (3)$$

where W_{im} is the neighborhood weight computed at pixel *i* for cluster *m*, and is governed by:

$$W_{im} = \frac{\sum_{q=1}^{Q} z_{q_i m}}{Q} \quad (4)$$

where *Q* is the number of pixels in a set of neighborhood of the *i*th pixel, and q_i denotes the *q*th neighbor's concentration value of the *i*th pixel. The neighbor pixels were selected to be of a window of size 3 x 3 with the current pixel in the window center at the window coordinate (2, 2).

These posterior probabilities are then used in the M-step to obtain "new" values θ using the following re-estimation formulas:

$$\pi_m = \frac{1}{N} \sum_{i=1}^{N} z_{im} \quad (5)$$

$$\mu_{X,m} = \frac{\sum_{i=1}^{N} z_{im}\, X(i)}{\sum_{i=1}^{N} z_{im}} \quad (6)$$

$$\Sigma_{X,m} = \frac{\sum_{i=1}^{N} z_{im} \left(X(i) - \mu_{X,m}\right)\left(X(i) - \mu_{X,m}\right)^T}{\sum_{i=1}^{N} z_{im}} \quad (7)$$

With this step, each pixel is represented by a group of cluster centers (*m* cluster centers), with *m* association values to these clusters. Then, CAM proceeds by isolating the pure-volume clusters away from the partial-volume clusters through detecting the vertices ("corners") of the convex hull that contains all the clusters. Each corner cluster represents the normalized time concentrations (TCs) of a single compartment, and these corner clusters represent the $\mathbb{a}$ term in (1), where $\mathbb{a} = \{\mathbb{a}_1, \mathbb{a}_2, \dots, \mathbb{a}_J\}$ and *J* is the total number of pure-volume compartments.

After determining the pure-volume pixels, then CAM has the probabilistic pixel memberships associated with the pure-volume compartments, z_{ij} for $j = 1, \dots, J$ and $i = 1, \dots, N$. Plasma Concentration, C_p, is associated with the cluster of the fastest enhancement (reaching its peak most rapidly); C_j (fast and slow flow concentrations) is associated with the cluster of *j*th tissue type. So, CAM computes C_p and C_j by:

$$C_p = \frac{\sum_{i=1}^{N} z_{ij}\, C_{measured}\ (i)}{\sum_{i=1}^{N} z_{iJ}}, C_j = \frac{\sum_{i=1}^{N} z_{ij}\, C_{measure\ d}(i)}{\sum_{i=1}^{N} z_{ij}} \quad (8)$$

for $j = 1, \dots, J-1$, where $C_{measured}\ (i)$ is the concentration at pixel *i*.

B. Barycentric Coordinate System

The clusters inside the convex hull – non-corner clusters- are considered of pixels with partial volume effect, where each pixel concentration value in these clusters is a mix of two or more of the pure-volume concentration values, and could be expressed through:

$$X(k) = \sum_{j=1}^{J} \alpha_j(k) C_j \quad (8)$$

where $k \in K = \{\{1,2, \dots, N\} \setminus P\}$, P is the set of pure-volume pixels identified by CAM till this step, α_j is the weight of the partial contribution of each pure-volume tissue C_j, and

$$\sum_{j=1}^{J} \alpha_j(k) = 1. \quad (9)$$

In geometry, the barycentric coordinate system (BCS) is a coordinate system in which the location of a point in a simplex (triangle, tetrahedron, etc.) is specified as the center of mass of other masses placed at its vertices (corners). Relying on the simplex constructed by CAM, we can get the contribution of each corner (pure-volume pixels) at each partial-volume pixel inside the convex hull. The coefficients α_j are called the barycentric coordinate system of the CAM simplex. The barycentric coordinate is not unique, but if the coefficients are restricted by (9), it will be unique [7].

Here is a simple example of getting the BCS for a triangular simplex with each data point is a sample of the space $\mathbb{R}^2$ in a Cartesian coordinate system (*x*, *y*). Suppose a point inside the simplex is $P = (x, y)$, and the triangle vertices are $C_i = (x_i, y_i),\ i \in \{1,2,3\}$, then

$$x = \alpha_1 x_1 + \alpha_2 x_2 + \alpha_3 x_3 \quad (10)$$

$$y = \alpha_1 y_1 + \alpha_2 y_2 + \alpha_3 y_3 \quad (11)$$

Substituting $\alpha_3 = 1 - \alpha_1 + \alpha_2$ in the above two equations, and rearrange:

$$\alpha_1(x_1 - x_3) + \alpha_2(x_2 - x_3) = x - x_3 \quad (12)$$

$$\alpha_1(y_1 - y_3) + \alpha_2(y_2 - y_3) = y - y_3 \quad (13)$$

This could be written in a more compact linear transformation as:

$$H.\alpha = P - C_3 \quad (14)$$

where H is given by:

$$H = \begin{pmatrix} (x_1 - x_3) & (x_2 - x_3) \\ (y_1 - y_3) & (y_2 - y_3) \end{pmatrix} \quad (15)$$

The matrix H is invertible since $C_1 - C_3$ *and* $C_2 - C_3$ are linearly independent to form a triangle. So,

$$\begin{pmatrix} \alpha_1 \\ \alpha_2 \end{pmatrix} = H^{-1}(P - C_3) \quad (16)$$

$$\alpha_3 = 1 - \alpha_1 + \alpha_2 \quad (17)$$

But for our case, where each data point is a sample of the space $\mathbb{R}^L$, where L is the total number of sampling time points, and is contaminated with some noise, the Alphas could be obtained by solving the optimization problem:

$$\hat{\alpha}(k) = \arg \min_{\alpha(i)} \|C_{measur\ ed}(k) - \mathbb{C}.\alpha(k)\|_2 \quad (18)$$

s.t. $0 \leq \alpha_j \leq 1$ and $\sum_{j=1}^{J} \alpha_j = 1$, where $C_{measured}\ (k)$ is the concentration at pixel k, and $\mathbb{C} = \{C_1, \ldots, C_{J-1}, C_p\}$ is the Time Activity Curves (TACs) of the tissue types estimated by the original CAM algorithm based on the pure-volume pixels on the convex hull vertices.

The above technique is applied on all pixels (CAM-identified pure-volume and partial-volume pixels). This could have a two-fold purpose. First, the estimated alphas, $\hat{\alpha}(k)$, could point out the pure-volume pixels that CAM misses by extracting those pixels having very high contribution from one compartment and almost negligible contributions from the remaining compartments. By this, the CAM problem of underestimating the true number of pure-volume pixels could be solved, or at least enhanced if the BCS could not accurately determine the remaining pure-volume pixels. Second, the CAM-identified pure-volume pixels are tested to keep those strongly belonging to one compartment and discard the others. This could overcome the CAM overestimation problem.

Then, TACs are recomputed via (8) using the pure-volume pixels determined by CAM and the BCS. The CAM then proceeds and computes the pharmacokinetic parameters K_j^{trans} *and* $k_{ep,j}$, *for* $j = 1, \ldots, J-1$.

III. Results and Discussion

To validate the proposed technique, a set of simulated DCE-MRI time series are synthesized by multiplying predefined local volume transfer constant maps $K^{trans}\ (i)$ by known compartment TCs $(k_{ep,f}, k_{ep,s}, C_p)$. Four different scenarios were obtained based on the different kinetic parameter values shown in Table I. The sampling rate was $t_l = 0.5(l-1)$, where l is the number of the sampling time points (18 points). A zero-mean Gaussian perturbation term and a zero-mean Gaussian noise were added to account for object variability and experimental noise, respectively. Results are repeated 10 times to check for accuracy (biasing) and reproducibility (variability).

The results on the pharmacokinetic parameters values (not shown for space considerations) computed by the original CAM and by CAM with the neighborhood weighted SFNM enhancement (NWCAM) are that, out of 48 values (4 parameters of 4 scenarios, each with 3 different noise levels), NWCAM outperformed in 26 cases, CAM outperformed in 22 cases, from which 9 ones are within an error of 5 % relative to the CAM values. The Root Mean Square Error (RMSE: mean ± variance) for CAM is 0.05409 ± 0.00496 and for NWCAM is 0.02926 ± 0.00187, which means that NWCAM is more accurate and more stable.

As for the results (not shown) of CAM and CAM with the Barycentric Coordinate System (BCAM), out of 48 cases, BCAM outperformed CAM in all the cases. The RMSE for BCAM is 0.01689 ± 0.000819.

After combining the two modifications of BCAM and NWCAM into BNWCAM, we obtained the results found in Table I. The RMSE for BNWCAM is 0.00348 ± 0.000019. The last RMSE value says that BNWCAM has the most accurate and stable values compared to CAM, NWCAM, and BCAM. In particular, the RMSE for the estimation of K_s^{trans} is 0.01748 ± 0.0004251 for CAM and 0.00069 ± 0.0000009 for BNWCAM; of $k_{ep,s}$ is 0.06246 ± 0.0018024 for CAM and 0.00194 ± 0.0000009 for BNWCAM; of K_f^{trans} is 0.11802 ± 0.0004611 for CAM and 0.02949 ± 0.0000005 for BNWCAM; and of $k_{ep,f}$ is 0.08421 ± 0.0088077 for CAM and 0.00662 ± 0.0000085 for BNWCAM.

Fig. 1(a) is the ground truth for the TCs of scenario 2 with SNR = 15 dB. CAM produced the TCs shown in Fig. 1(b), while Fig. 1(c) shows those of BNWCAM. It could be seen that BNWCAM TCs are closer to the ground truth curves.

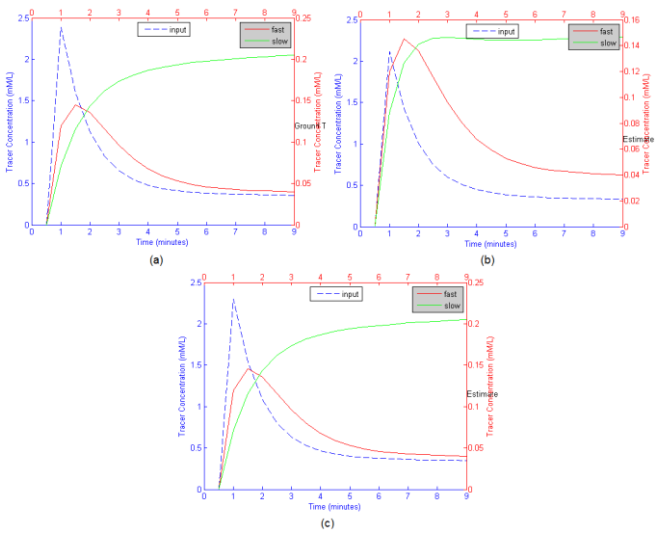

Figure 1. Time concentration curves (TCs) of scenario 2 with SNR = 15 dB. (a) The ground truth TCs. (b) TCs after applying CAM. (c) TCs after applying BNWCAM.

The ground truth numbers of pure volume pixels for the three compartments are 159, 99, and 315 pixels. Table II shows the number of pixels defined as pure-volume pixels after applying CAM and BNWCAM. These numbers indicate that BNWCAM has less variability in the number of pure-volume pixels at looking at it either horizontally (the same

scenario with different noise levels) or vertically (the same tissue types, but with different kinetic parameter values), which means more robustness for determining the pure-volume pixels and independency of noise and of kinetic parameters pattern.

TABLE I. KINETIC PARAMETER VALUES ESTIMATED BY CAM AND BNWCAM

Ground Truth		SNR = 10		SNR = 15		SNR = 20	
		CAM	BNWCAM	CAM	BNWCAM	CAM	BNWCAM
Scenario 1	K_s^{trans} = 0.03 /min	0.0321	0.0302	0.0291	0.0303	0.0281	0.0303
	$k_{ep,s}$ = 0.1 /min	0.0934	0.0971	0.1571	0.1002	0.1593	0.1005
	K_f^{trans} = 0.03 /min	0.0313	0.0299	0.0307	0.0303	0.03	0.0303
	$k_{ep,f}$ = 0.5 /min	0.4626	0.4877	0.4866	0.5009	0.5002	0.5014
Scenario 2	K_s^{trans} = 0.03 /min	0.0288	0.0298	0.0337	0.0300	0.0292	0.0300
	$k_{ep,s}$ = 0.1 /min	0.0972	0.0962	0.1966	0.0995	0.1849	0.0999
	K_f^{trans} = 0.05 /min	0.0475	0.0498	0.0579	0.0500	0.0499	0.0499
	$k_{ep,f}$ = 1.2 /min	1.1628	1.1886	1.2620	1.1988	1.1977	1.1976
Scenario 3	K_s^{trans} = 0.06 /min	0.0798	0.0621	0.1082	0.0610	0.0615	0.0600
	$k_{ep,s}$ = 0.5 /min	0.6227	0.4978	0.5339	0.5023	0.5036	0.5008
	K_f^{trans} = 0.05 /min	0.0713	0.0517	0.0923	0.0509	0.0512	0.0500
	$k_{ep,f}$ = 1.2 /min	1.2470	1.19144	1.3294	1.2044	1.2075	1.2015
Scenario 4	K_s^{trans} = 0.05 /min	0.0494	0.0499	0.0760	0.0503	0.0658	0.0500
	$k_{ep,s}$ = 0.6 /min	0.5156	0.5977	0.6026	0.5976	0.6099	0.6002
	K_f^{trans} = 0.08 /min	0.0783	0.0796	0.1235	0.0806	0.1064	0.0800
	$k_{ep,f}$ = 1.5 /min	1.2696	1.5118	1.5595	1.5005	1.5515	1.4997

TABLE II. STANDARD DEVIATION OF THE NUMBER OF PURE-VOLUME PIXELS ESTIMATED BY CAM AND BNWCAM

	SNR = 10		SNR = 15		SNR = 20			
	CAM	BNWCAM	CAM	BNWCAM	CAM	BNWCAM		
S1	317	573	858	577	956	576	344.14	2.08
S2	317	573	925	573	955	574	360.00	0.57
S3	500	580	444	579	549	573	52.53	3.78
S4	469	519	342	576	577	573	117.62	32.07
	97.53	28.35	292.08	2.5	226.89	1.41		

In addition, the differences between the estimated pure-volume pixels by CAM and BNWCAM in Table II shows the ability of the two reported enhancements to overcome, to a very satisfactory level, the two CAM problems of underestimating and overestimating the accurate number of pure-volume pixels, which has a direct reflection on the accuracy of parameters estimation as shown in Table I and as reported in the RMSE values.

Also, the proposed technique was applied on typical breast DCE-MRI case. The TCs are shown in Fig. 2 for CAM, Fig. 2(a), and for BNWCAM, Fig. 2(b). As for the numbers of pure-volume pixels identified by CAM, they are 15, 50, and 83 for the three tissue compartments; and they are 57, 169, and 170 for BNWCAM.

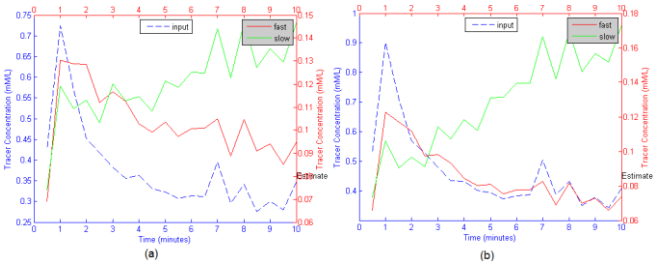

Figure 2. TCs for a typical breast DCE-MRI case. (a) CAM. (b). BNWCAM.

IV. CONCLUSION

This paper provides an enhanced version of the CAM-CM technique used to estimate the pharmacokinetic parameters in the DCE-MRI images based on isolating and determining the pure-volume pixels and ignoring the pixels with PVE. The enhancement comes in the use of barycentric coordinate system to test the pixels classified by CAM to get an accurate estimate of the pure-volume pixels, , after introducing the neighborhood effect around each pixel on that pixel. Results show more accuracy and robustness over the conventional CAM technique.

REFERENCES

[1] James P. B. O'Connor, Alan Jackson, Geoff J. M. Parker, Caleb Roberts, and Gordon C. Jayson, "Dynamic contrast-enhanced MRI in clinical trials of antivascular therapies," *Nature Reviews in Clinical Oncology*, vol. 9, pp. 167–177, 2012.

[2] SP Sourbron and DL Buckley, "Tracer kinetic modelling in MRI: estimating perfusion and capillary permeability," Phys. Med. Biol. Vol. 57, 2012.

[3] Hatef Mehrabian, Rajiv Chopra, and Anne L. Martel, "Calculation of Intravascular Signal in Dynamic Contrast Enhanced-MRI Using Adaptive Complex Independent Component Analysis," *IEEE Trans. Medical Imaging*, vol. 32, no. 4 pp. 600-710, April 2013.

[4] Daniel Rodriguez Gutierrez, Oliver Diaz Montesdeoca, Acerina Moran Santana, Kevin Wells, Iosif Mendichovszky, and Isky Gordon, "MR-based renography as a replacement for radionuclide diagnostic studies," *IEEE Nuclear Science Symposium Conference*, Hawaii, USA 2007, pp. 4556 - 4563.

[5] Li Chen, Peter L. Choyke, Tsung-Han Chan, Chong-Yung Chi, Ge Wang, and Yue Wang, "Tissue-Specific Compartmental Analysis for Dynamic Contrast-Enhanced MR Imaging of Complex Tumors," *IEEE Trans. Medical Imaging*, vol. 30, no. 12, pp. 2044-2058, December 2011.

[6] Hui Tang, Jean-Louis Dillenseger, and Li Min Luo, "A Vectorial Image Classification Method Based On Neighborhood Weighted Gaussian Mixture Model," *Proc. of the 30th Conf. IEEE-EMBS*, Vancouver, British Columbia, Canada, August, 2008, pp. 1922-1925.

[7] Wenli Cai, Se Hyung Kim, June-Goo Lee, and Hiroyuki Yoshida, "Virtual Colon Tagging for Electronic Cleansing in Dual-energy Fecal-tagging CT Colonography," *Proc. of the 34th Conf. IEEE-EMBS*, San Diego, California USA, 28 August - 1 September, 2012, pp. 3736-3739.